

# Reliability assessment on interfacial failure of thermal barrier coatings

Jin-Wei Guo<sup>1,2</sup> · Li Yang<sup>1,2</sup> · Yi-Chun Zhou<sup>1,2</sup> · Li-Min He<sup>3</sup> · Wang Zhu<sup>1,2</sup> · Can-Ying Cai<sup>1,2</sup> · Chun-Sheng Lu<sup>4</sup>

Received: 30 August 2015 / Revised: 15 December 2015 / Accepted: 25 May 2016 / Published online: 23 August 2016

© The Chinese Society of Theoretical and Applied Mechanics; Institute of Mechanics, Chinese Academy of Sciences and Springer-Verlag Berlin Heidelberg 2016

**Abstract** Thermal barrier coatings (TBCs) usually exhibit an uncertain lifetime owing to their scattering mechanical properties and severe service conditions. To consider these uncertainties, a reliability assessment method is proposed based on failure probability analysis. First, a limit state equation is established to demarcate the boundary between failure and safe regions, and then the failure probability is calculated by the integration of a probability density function in the failure area according to the first- or second-order moment. It is shown that the parameters related to interfacial failure follow a Weibull distribution in two types of TBC. The interfacial failure of TBCs is significantly affected by the thermal mismatch of material properties and the temperature drop in service.

**Keywords** Reliability assessment · Thermal barrier coatings · Interfacial failure

✉ Li Yang  
lyang@xtu.edu.cn

✉ Yi-Chun Zhou  
zhouyc@xtu.edu.cn

<sup>1</sup> Key Laboratory of Key Film Materials & Application for Equipment (Hunan Province), School of Materials Science and Engineering, Xiangtan University, Xiangtan 411105, China

<sup>2</sup> Key Laboratory of Low Dimensional Materials & Application Technology (Ministry of Education), School of Materials Science and Engineering, Xiangtan University, Xiangtan 411105, China

<sup>3</sup> Beijing Institute of Aeronautical Materials, Beijing 100095, China

<sup>4</sup> Department of Mechanical Engineering, Curtin University, Perth, Western Australia 6845, Australia

## 1 Introduction

The performance of a gas turbine relies heavily on the thrust–weight ratio, whose continuous improvement results in a constant increase of gas temperature. Nowadays, the gas temperature in aircraft turbines reaches as high as 1600 °C. However, the maximum operational temperature of refractory Ni-base superalloys used for high-temperature components is approximately 1100 °C, which approaches their service limit [1]. To protect structural materials from hot gases, thermal barrier coatings (TBCs) have been widely used owing to their excellent thermal protection, high hardness, and wear resistance [2–4]. Generally, TBCs comprise an yttria-stabilized zirconia ceramic layer that keeps hot gases from melting and then protects components, a substrate that endures mechanical loading and an MCrAlY alloy (M represents Ni, Co, or Fe) bond-coating that enhances the adhesion of the ceramic coating to a substrate. During processing and further thermal exposure, the fourth layer, known as a thermally grown oxide (TGO), is formed between the bond and top coatings owing to the diffusion and reaction of oxygen and metal ions. Moreover, the interface structure of multi-layered TBCs and the shape of protected components, such as turbine blades and vanes, are very complex. Under extremely high temperatures coupled with oxidation, erosion, and corrosion, TBCs suffer primarily from the cleavage and spallation of ceramic coatings [2–6]. To ensure safety and take advantage of TBCs, it is necessary to develop a reliable analytical model to predict their lifetime.

Significant efforts have been dedicated to predict the lifetime of TBCs. For instance, Busso et al. [7,8] revealed that damage in TBCs mainly depended on stress (perpendicular to the interface) between the ceramic coating and

TGO, which can be determined by finite-element simulations. Based on a continuum damage mechanics model, the researchers established a physics-based life prediction method [8]. The evolution of damage parameters, such as the cumulative acoustic emission energy [9], crack length [10], crack density [11], and damage area [12], was monitored in real time to analyze the residual life of TBCs. He et al. [13] proposed a life prediction model based on fracture mechanics, in which cracks were assumed to occur in a ceramic coating under tension once the energy release rate reached its fracture toughness. The growth of TGO is widely considered a key factor in the failure of TBCs, and several life prediction models have been developed based on the thickness of TGOs and strain in ceramic coatings [14, 15]. Obviously, these models provide guidance on the service period of TBCs; however, their applications are limited by the lack of consideration of the uncertainty of material properties and service conditions.

Owing to the brittle nature, numerous pores, and microcracks with different sizes in its microstructure, the properties of a ceramic coating (e.g., Young's modulus, strength, fracture toughness, and thermal expansion coefficient) vary widely [16, 17]. In addition, the variations and uncertainties are also present in the geometry and loading conditions. For example, a rough interface appears between the ceramic and bond coating with various wavelengths and amplitudes in different regions, indicating a substantial amount of scatter in the adhesion strength of the interface. After a period of high-temperature oxidation, the thickness, microstructure, and shape of TGOs unavoidably vary within certain limits [17], resulting in inconstant strength and elastic modulus. More importantly, TBCs suffer from a changing temperature with or without erosion (and corrosion) by foreign particles. Thus, the nonuniform parameters, microstructures, and variable operation conditions can result in a dispersive service life of TBCs. Therefore, traditional life criteria, such as maximum stress or other damage parameter, are deficient because they are only based on the mean value of the load or strength. The uncertainties, which relate to the reliability of TBC performance under variable service conditions, need to be quantified.

As shown in Fig. 1, there are three main failure types in TBCs: cleavage of ceramic coating, spallation within ceramic coating, and spallation of ceramic coating along ceramic/bond or TGO interface [18, 19]. The cleavage of a ceramic coating, resulting from cracks that are vertical to interfaces activated by tensile stress in coating owing to a thermal mismatch, sintering, or phase transformation, supplies an entrance for oxygen and thermal diffusion, and thus degrades the thermal insulation performance of coatings. Spallation within a ceramic coating is mainly induced by the erosion or corrosion of molten calcium-magnesium-alumina-silicate mixtures, which decreases the thickness of

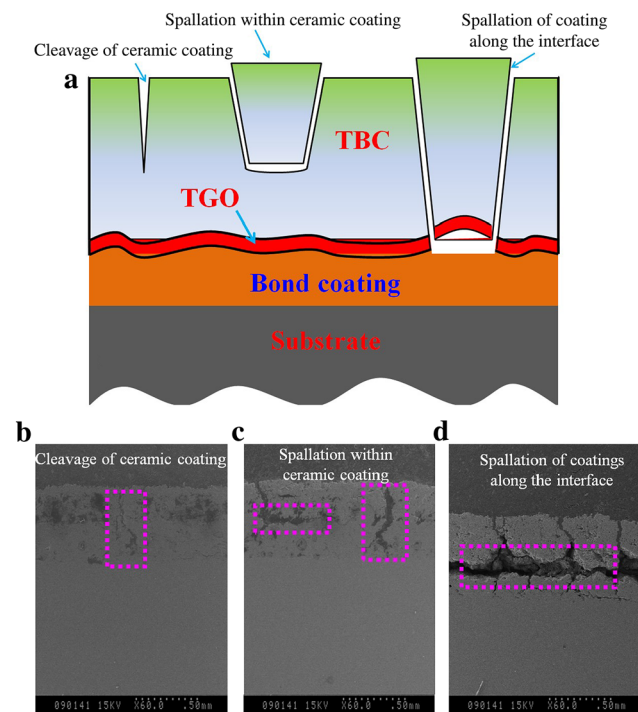


**Fig. 1** a Schematic of three types of failure mode in TBCs: cleavage of ceramic coating, spallation in ceramic coating, and spallation at interface. Scanning electron microscopy images of TBCs indicate **b** cleavage failure, **c** spallation in ceramic coating, and **d** spallation at interface, respectively

the thermal insulation layer [20, 21]. However, spallation on a ceramic/bond or TGO interface is very dangerous because of the loss of the thermal insulation layer. Therefore, the prediction of spallation at interfaces is especially crucial in a reliability assessment of TBCs.

Taking into account the scatter of the material properties, uncertain loading conditions, and geometrical variations, current research has focused on a reliability assessment method in quantifying the risk of interface spallation in TBCs. The main idea behind such a method is to analyze the failure probability of TBCs based on a first- or second-order algorithm. To distinctly identify failure, a limit state equation is established to demarcate a boundary between failure and safe regions. Then, factors relevant to failure and their distributions are analyzed. Finally, the failure probability and sensibility of influence factors are calculated. In this paper, a description of this method is given in Sect. 2. Section 3 is dedicated to the distributions of key parameters that influence the interfacial failure of TBCs and experimental verification. Owing to their different properties, microstructures, and interface shapes, two types of TBC are prepared. The reliability assessment of spallation at interfaces is discussed in Sect. 4. Finally, a brief summary is given.

## 2 Reliability assessment method

### 2.1 Failure probability

To assess the reliability and predict the lifetime of a material (or structure), a boundary needs to be determined that separates the design space into failure and safe regions. A boundary based on a simplified model consists of two variables: strength or resistance  $R$  and load  $S$ . Mathematically, this is referred to as a limit state function,

$$Z = R - S = 0. \tag{1}$$

It is obvious that  $Z > 0$  indicates that the material is in a safe state. However,  $Z < 0$  and  $Z = 0$  represent its failure region and critical state, respectively. Generally, the limit state function is often formulated as a function of all relevant load and resistance parameters, called basic or random variables  $X_i$  (e.g., load, material properties), that is,

$$Z(X_1, X_2, X_3, \dots, X_n) = 0, \tag{2}$$

where the performance function  $Z(X)$  ( $X = (X_1, X_2, X_3, \dots, X_n)$ ) is commonly nonlinear. The failure probability can be obtained by

$$\begin{aligned} P_f &= \int_{-\infty}^0 f_Z(z) dz \\ &= \int \dots \int_{\Omega} f_X(X_1, X_2, X_3, \dots, X_n) dX_1 dX_2 \dots dX_n, \end{aligned} \tag{3}$$

in which  $f(X_1, X_2, X_3, \dots, X_n)$  is the joint probability density function of  $X$ , and the integration is performed over the failure region  $\Omega$  with  $Z \leq 0$ . Assuming the variables  $X_i$  are independent, the joint probability density function can be replaced by individual density functions:

$$P_f = \int \dots \int_{\Omega} f_{X_1}(X_1) f_{X_2}(X_2) \dots f_{X_n}(X_n) dX_1 dX_2 \dots dX_n. \tag{4}$$

These individual density functions, as well as the solution of this multiple integral are, in general, extremely difficult to determine. In the case of TBCs, there are different limit state functions with a huge number of random variables that are associated with various failure modes. Therefore, the failure probability can be only determined using other approximate and efficient methods [22–27].

Obviously, a failure probability is dependent on the performance function  $Z$ . Assuming  $Z$  satisfies a normal distribution with a mean of  $\mu_Z$  and a standard deviation of  $\sigma_Z$ , its probability density function can be described as

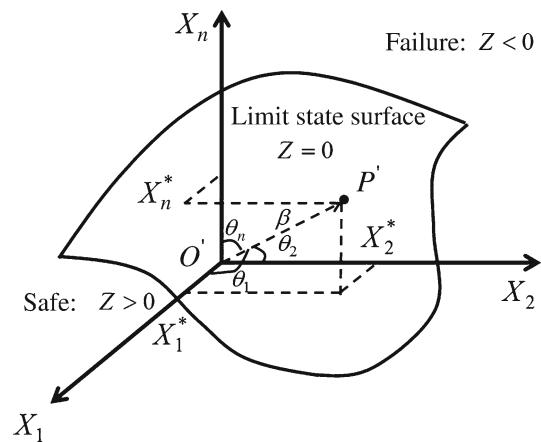


Fig. 2 Illustration of limit state surface in an  $n$ -dimensional space with  $n$  random variables

$$f_Z(Z) = \frac{1}{\sqrt{2\pi}\sigma_Z} \exp\left[-\frac{(Z - \mu_Z)^2}{2\sigma_Z^2}\right]. \tag{5}$$

By introducing  $Z' = \frac{Z - \mu_Z}{\sigma_Z}$  (the zero mean and unit variance), the failure probability can be expressed as

$$\begin{aligned} P_f &= \int_{-\infty}^0 f_Z(Z) dZ \\ &= \int_{-\infty}^{-\frac{\mu_Z}{\sigma_Z}} \frac{1}{\sqrt{2\pi}} \exp\left(-\frac{Z'^2}{2}\right) dZ' \\ &= \int_{-\infty}^{-\frac{\mu_Z}{\sigma_Z}} \varphi(Z') dZ' \\ &= \Phi\left(-\frac{\mu_Z}{\sigma_Z}\right) = \Phi(-\beta), \end{aligned} \tag{6}$$

where  $\Phi()$  and  $\varphi()$  are the standard normal cumulative distribution and probability functions, respectively. The ratio  $\beta$  of the mean value to standard deviation of  $Z$  is defined as the reliability index. In the  $n$ -dimensional space with  $n$  random variables (Fig. 2),  $\beta$  can also be interpreted as the minimum distance between the original point (the mean point of a performance function  $Z$ ) and the failure surface in a standard normal space. Consequently,  $\beta$  may be regarded as a safety margin, indicating how far the system is from failure when it is in its mean state. The design point  $X^*$  (closest to the mean point) yields the highest risk of failure among all points on the failure surface.

### 2.2 First-order second moment reliability

The determination of the design point  $\beta$  is a constrained nonlinear minimization problem. It is obvious that Eq. (6) is accurate only if the performance function  $Z'$  is a normal distribution with a mean of zero and a standard deviation of one.

This indicates that the elements of  $X$  are standardized normal variables and the failure surface is a hyperplane, where  $Z$  is a linear function of its random variables. These conditions are rarely met in applications. Therefore, the advanced first-order second moment reliability method is developed to deal with these two problems. Its main idea is to transform all random variables  $(X_1, X_2, X_3, \dots, X_n)$  to the space of standard normal variables  $(X'_1, X'_2, X'_3, \dots, X'_n)$ , and meanwhile to linearize the nonlinear performance function  $Z$  by expanding it as a first-order Taylor series. Based on the idea of equivalent normalization conditions, the cumulative distribution function of  $X_i$  is equal to that of  $X'_i$ , and the standardized forms of  $X_i$  can be represented as

$$X'_i = \begin{cases} \frac{X_i - \mu_{X_i}}{\sigma_{X_i}} X_i, & \text{is a normal variable,} \\ \Phi^{-1}(F_{X_i}(X_i)) X_i, & \text{is not a normal variable,} \end{cases} \quad (7)$$

where  $F_{X_i}()$  is the cumulative distribution function for  $X_i$ , and the definition of  $\Phi()$  is the same as that in Eq. (6).  $X'_i$  and  $X_i$  are the standard normal variables and random variables, respectively. The subscript  $i$  represents the number of parameters ( $i = 1, 2, 3, \dots, n$ ). Adapting the standard variables, the limit state equation can be written in terms of the standardized variables as

$$Z(X_1, X_2, X_3, \dots, X_n) = G(X'_1, X'_2, X'_3, \dots, X'_n) = 0. \quad (8)$$

The nonlinear performance function  $G$  is also expanded by a first-order Taylor series at the original test point  $X^0$ , that is,

$$G(X') = G(X^0) + \sum_{i=1}^n \frac{\partial G(X^0)}{\partial X'_i} (X'_i - X'^0_i), \quad (9)$$

and then the expected (mean) value and standard deviation of  $G(X')$  are given by

$$\mu_{G_0} = G(X^0) - \sum_{i=1}^n \frac{\partial G(X^0)}{\partial X'_i} X'^0_i \quad (10)$$

and

$$\sigma_{G_0} = \sqrt{\sum_{i=1}^n \left( \frac{\partial G(X^0)}{\partial X'_i} \right)^2}. \quad (11)$$

The corresponding reliability index  $\beta$  can be expressed as

$$\beta = \frac{\mu_{G_0}}{\sigma_{G_0}}. \quad (12)$$

In the space of a standard normal variable  $X'$ , the function  $G = 0$  represents the tangent plane of a limit state surface at

point  $X^0$ . According to the geometrical definition of  $\beta$ , the design point  $X'^*$  at the standard variable space can be found by the following constrained optimization problem by minimizing  $\beta = (X'^T X')^{1/2}$  subject to the constraint  $G(X') = 0$ . Defining a parameter as

$$\cos \theta_{X'_i} = - \frac{\frac{\partial G(X')}{\partial X'_i}}{\sqrt{\sum_{i=1}^n \left( \frac{\partial G(X')}{\partial X'_i} \right)^2}} \quad (13)$$

it describes the relative influence of the  $i$ -th element on the standard deviation of  $G$ . The new test point closing to the design point is obtained by

$$X'_i = \beta \cos \theta_{X'_i}. \quad (14)$$

The algorithm to compute  $\beta$  and the design point  $X^*$  of TBCs can be formulated as follows:

- (1) Define an appropriate limit state equation.
- (2) Ascertain the influential variables  $X_i$  ( $i = 1, 2, \dots, n$ ), analyze their distributions, and then obtain standardized normal forms according to Eq. (7).
- (3) Assume initial values of  $X'^0_i$ , which are typically assumed to be the mean values of these random variables.
- (4) Evaluate the approximate moment of a performance function  $G$  by the first-order Taylor series, its corresponding reliability index  $\beta$ , and direction cosine  $\cos \theta_{X'_i}$ , as mentioned in Eqs. (9), (12), and (13), respectively.
- (5) Express a new test point  $X'$  in terms of Eq. (14), and substitute the new  $X'$  for the initial values of  $X^0$  at step 3.
- (6) Repeat steps 4 and 5 until  $\beta$  converges. Then the failure probability of TBCs can be evaluated by Eq. (6) with the obtained  $\beta$ .

### 2.3 Second-order second moment reliability

When the higher-order terms of a Taylor series cannot be neglected, significant error may be introduced in a first-order approximation method. With the advantage of the concave, convex, curvature, and other nonlinear properties of the failure surface, the second-order second moment reliability method can be used to improve the accuracy [28]. The principle of this method is to expand the nonlinear performance function at the design point  $X'^*$  by retaining the second-order terms, that is,

$$G(X') = G(X'^*) + \nabla G(X'^*)^T (X' - X'^*) + \frac{1}{2} (X' - X'^*)^T \nabla^2 G(X'^*)^T (X' - X'^*), \quad (15)$$

where

$$\nabla G(\mathbf{X}^{j*}) = \left( \frac{\partial G(\mathbf{X}^{j*})}{\partial X_1^j}, \frac{\partial G(\mathbf{X}^{j*})}{\partial X_2^j}, \dots, \frac{\partial G(\mathbf{X}^{j*})}{\partial X_n^j} \right)^T.$$

Next, let us define the unit vector and matrix as

$$\alpha_{\mathbf{X}^{j*}} = - \frac{\nabla G(\mathbf{X}^{j*})}{\|\nabla G(\mathbf{X}^{j*})\|} \tag{16}$$

and

$$\mathbf{Q}_{\mathbf{X}^{j*}} = - \frac{\nabla G^2(\mathbf{X}^{j*})}{\|\nabla G(\mathbf{X}^{j*})\|}, \tag{17}$$

where

$$\|\nabla G(\mathbf{X}^{j*})\| = \sqrt{\sum_{i=1}^n \left( \frac{\partial G(\mathbf{X}^{j*})}{\partial X_i^j} \right)^2}.$$

Based on the orthogonal normalization processing technique, an orthogonal matrix  $\mathbf{H}$  can be constructed based on the unit vector  $\alpha_{\mathbf{X}^{j*}}$ , which is located in the  $n$ -th row of the matrix. Then the second-order failure probability can be expressed as [29]

$$P_f = \frac{\Phi(-\beta)}{\sqrt{\det[\mathbf{I} - \beta(\mathbf{H}^T \mathbf{Q} \mathbf{H})_{n-1}]}} \tag{18}$$

where  $\beta$  is the reliability index determined in the advanced first-order second moment reliability method.

Based on the first-order second moment reliability method, the second-order failure probability can be obtained by the following steps:

- (1) According to the method mentioned by Sect. 2.2, the corresponding reliability index  $\beta$  can be obtained (see Eqs. (8)–(14)).
- (2) Define an appropriate limit state equation, and expand the nonlinear performance function at the design point  $\mathbf{X}^{j*}$  by retaining second-order terms according to Eq. (15).
- (3) Obtain the unit vector  $\alpha_{\mathbf{X}^{j*}}$  and matrix  $\mathbf{Q}_{\mathbf{X}^{j*}}$  according to Eqs. (16) and (17).
- (4) Construct the orthogonal matrix  $\mathbf{H}$  in terms of the orthogonal normalization processing technique.
- (5) Then the second-order failure probability can be obtained by Eq. (18).

### 2.4 Sensitivity analysis

To estimate the degree of influence of the change in random variables, a direct index is introduced to determine key factors

in the failure probability of TBCs. Based on the second-order fitting [30], the failure probability  $P_f$  of TBCs can be fitted by

$$P_f = aX_i^2 + bX_i + c, \tag{19}$$

where  $a$ ,  $b$ , and  $c$  are constants to be determined by the test data of variables and their corresponding failure probabilities  $(X_i^j, P_f^j)$  with weighted least-squares regression. In the case of  $j$  ranging from 1 to 5, the weight factors  $(\partial_1, \partial_2, \partial_3, \partial_4, \partial_5)$  are chosen as (1, 2, 4, 2, 1), and  $X_i^3$  is the reference point.

The sensitivity factor of variable  $X_i$  is obtained as

$$\begin{aligned} w_{P_{X_i}} &= \left| \frac{\partial P_f}{\partial X_i} \right|_{X_i=X_i^r} \times \frac{X_i^r}{P_f|_{X_i=X_i^r}} \times P_{X_i^r} \\ &= |2aX_i^r + b| \times \frac{X_i^r}{P_f|_{X_i=X_i^r}} \times P_{X_i^r}, \end{aligned} \tag{20}$$

where  $X_i^r$  is the reference point to the sensitivity of  $X_i$ , and  $P_{X_i^r}$  is the deviation probability of  $X_i$  to  $X_i^r$ .

### 3 Random variables and their distributions

As mentioned earlier, the interface crack as well as final delamination of the ceramic coating is mainly due to stresses that arise from thermal mismatches and the growth of an oxidation layer [31]. These stresses are affected by material properties, geometric factors, and loading conditions. Therefore, there are three kinds of variables in the probability analysis of interface failure: the interface strength or fracture toughness, external loads (e.g., temperature, thermal cycles), and the correlation of resistance and loads (e.g., Young’s modulus, thermal expansion coefficients, amplitude, and wavelength of TGO). To judge the boundary between safety and failure, one or more uncorrelated variables for each kind are included in a distinct limit state function. The measured material properties, including the modulus, strength, fracture toughness, Poisson’s ratio, and thermal expansion coefficient, show considerable scatters. It is found that the interface strength, hardness, elastic modulus, and fracture toughness can be well described by the Weibull distribution, while the thermal expansion coefficient and Poisson’s ratio show a normal distribution [16, 17]. The loading conditions and geometric properties, such as thickness, microstructures, and shapes of TGO, also present variations and uncertainties [17]. Obviously, these scattering features should be considered in a probabilistic analysis to quantify the probability of whether the performance of TBCs does not meet the service requirement, which is referred to as failure.

The distribution of a variable is commonly represented by a probability density function [29]. As a typical brittle coating material, the interface strength, modulus, and fracture

toughness can be well described by the Weibull distribution [32–34]. To confirm this distribution in TBCs, a compressive test was applied to trigger interface cracks and, thus, determine their resistance. Then the collected data are characterized using the Weibull distribution:

$$\ln\left(\frac{1}{1-P_f}\right) = m \ln\left(\frac{\sigma}{\sigma_0}\right) = m \ln \sigma - m \ln \sigma_0, \quad (21)$$

where  $P_f$  is the failure probability,  $m$  is the Weibull modulus or a shape parameter, and  $\sigma_0$  is the characteristic strength or a scale parameter. In Eq. (21),  $P_f$  can be estimated by

$$P_f = \frac{i - 0.5}{N}, \quad (22)$$

where  $i$  is the ordinal number of a measured fracture strength in ascending order of magnitude, and  $N$  is the total number of specimens [35].

A total of 12 TBC specimens are prepared by the air plasma spraying (APS) method and then measured under compression. The specimens consist of Ni-based superalloy GH3030 with a thickness of 5 mm, CoNiAlY bonding, and  $ZrO_2 - 8\%Y_2O_3$  ceramic coating with thicknesses of 100  $\mu\text{m}$  and 200  $\mu\text{m}$ . The length and width of the TBC specimens are 20 mm and 5 mm, respectively. The fracture strength is judged and determined by the acoustic emission response during compression at a loading rate of 250 N/min. Details on the compression tests and acoustic emission monitoring are given in our previous work [36]. As shown in Fig. 3, the Weibull distribution is best fitted for the measured data with a characteristic strength of 343.71 MPa and Weibull modulus of 21.91. Similar results were obtained for the Young's modulus [16] and fracture toughness [33,34] of TBCs. For other variables involved in the performance function, such as geometries (thickness, amplitude, and wavelength of TGO), material properties (thermal expan-

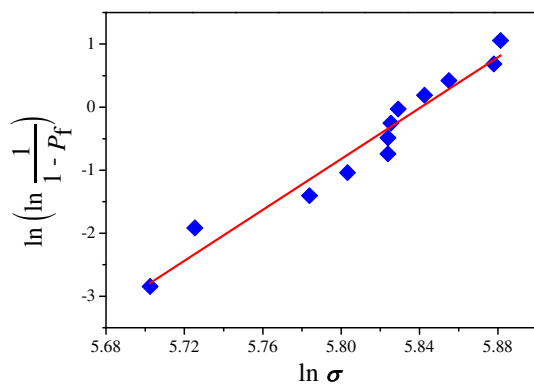


**Fig. 3** Measured results of interface strengths, showing a typical Weibull distribution with a characteristic strength of 343.71 MPa and Weibull modulus of 21.91

sion coefficients), and loads (temperature, thermal cycles), a normal distribution is assumed to be able to conveniently estimate the failure probability.

## 4 Interface failure probability

There are two methods to prepare TBCs on a substrate: APS and electron beam physical vapor deposition (EB-PVD). Catastrophic failure is due to the spallation of the ceramic coating induced by a thermal mismatch and TGO growth strain; however, spallation occurs at different locations in these TBCs because of their different microstructures.

### 4.1 TBCs by APS

APS ceramic coatings are multilayered with numerous pores, intersplat boundaries, and cracks parallel to the metal/ceramic interface. The ceramic/bond interface is rough and looks approximately like a periodic cosine wave with a certain amplitude and wavelength. He et al. [13] revealed that the spallation of an APS ceramic coating primarily appears at the intersplat boundary or cracks just above the rough ceramic/bond coating interface under compression. The corresponding delamination criterion (or limit state function) was established when the energy release rate  $G$  (for cracks in the ceramic coating to extend parallel to the interface) reaches the fracture toughness  $\Gamma_{\text{TBC}}$ . It can be represented as

$$Z = \Gamma_{\text{TBC}} - G = \Gamma_{\text{TBC}} - E_{\text{TBC}}L(\Delta\alpha\Delta T)^2\kappa(N - N_0) = 0, \quad (23)$$

where  $L$  is the half-wavelength of the TGO,  $E_{\text{TBC}}$  is the Young's modulus of the ceramic coating,  $\Delta\alpha$  is the difference in the thermal expansion coefficients between the substrate and ceramic coating,  $\Delta T$  is the temperature drop (taken to be positive),  $\kappa$  is a parameter relative to the strain growth induced by the TGO, and  $N$  is the number of thermal cycles when the interfacial delamination failure occurs. As shown in Table 1, the mean value of  $N$  is taken as 400.  $N_0$  is the

**Table 1** Parameters in probability analysis of TBCs produced by APS

Property	Mean value	Standard deviation	Distribution
$\Gamma_{\text{TBC}}$ (J/m <sup>2</sup> )	50	10	Weibull
$E_{\text{TBC}}$ (GPa)	40	8	Weibull
$L$ ( $\mu\text{m}$ )	20	4	Normal
$\Delta\alpha$ ( $10^{-6}/^\circ\text{C}$ )	4	0.2	Normal
$\Delta T$ ( $^\circ\text{C}$ )	1000	12	Normal
$\kappa$	0.009	0.002	Normal
$N$	400	20	Normal

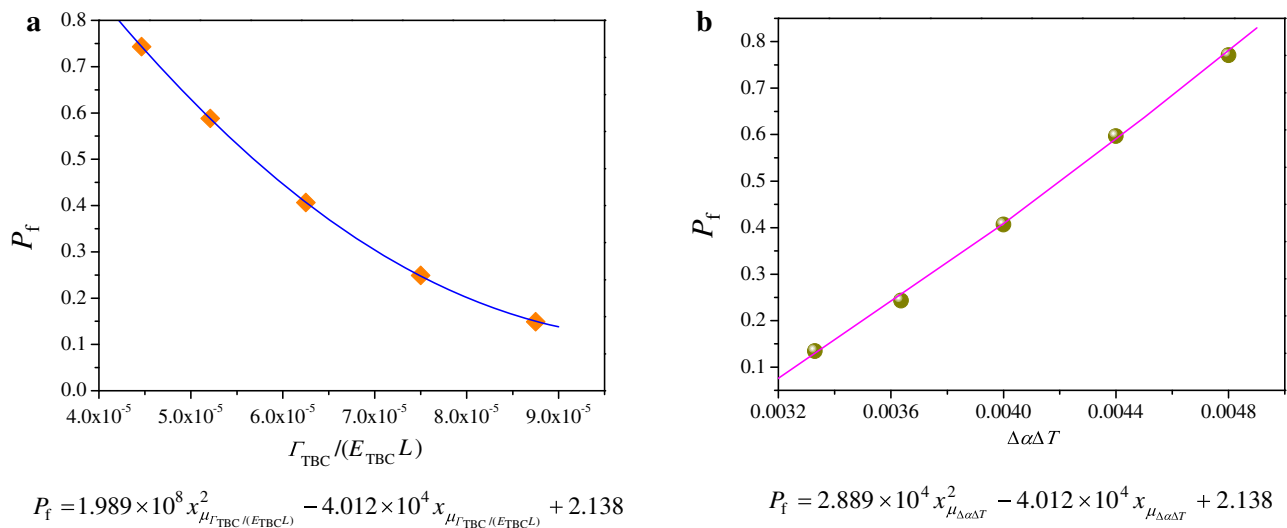


**Fig. 4** Curves of probability versus **a** nondimensional interface fracture toughness and **b** thermal strain of ceramic coating

critical number of thermal cycles, which means the minimum number of thermal cycles to cause failure.

Due to the high nonlinearity in Eq. (23), the failure probability is analyzed by employing the second-order second moment reliability method. First, the distribution of random variables and their mean values and deviations need to be ascertained. It is worth noting that the parameters in Table 1 can be determined by experimental results. Taking  $k$  as an example,  $k$  is a parameter relative to the strain growth induced by the TGO, which can be obtained by the relationship between the TGO thickness and oxidation time. Based on the discussion in Sect. 3, the Young’s modulus [16] and fracture toughness [33,34] of TBCs are Weibull variables, and their means and deviations can also be determined by experimental results [16,34].

Other involved variables, such as temperature drop, thermal expansion coefficient, wavelength of TGO, and  $k$ , are found to be normally distributed, with their mean values and deviations as listed in Table 1 [32]. Then all random variables in Eq. (23) are transformed into their equivalent standardized normal forms by Eq. (7). The transformation and risk quantification are realized with a MATLAB program. Using the values of the variables in Table 1, the failure probability is calculated as 40.64 %, indicating that the service conditions of the TBCs (e.g., temperature drop, thermal cycles) are dangerous.

The variation tendency of the failure probability can also be determined by changing the values of the variables. Figure 4 shows the curves of probability versus the nondimensional interface fracture toughness ( $\Gamma_{TBC}/(E_{TBC}L)$ ) of a ceramic coating. As expected, the risk probability decreases with increases in the nondimensional interface toughness  $\Gamma_{TBC}/(E_{TBC}L)$ , which means that the failure probability decreases with increases in resistance index (interface

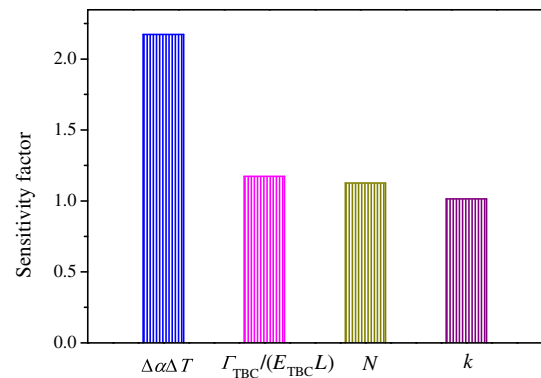


**Fig. 5** Sensitivity factors of nondimensional variables in spallation of APS ceramic coating

toughness), but it conversely increases with the rise of load-related parameters such as Young’s modulus. The relationship between the failure probability and  $\Gamma_{TBC}/(E_{TBC}L)$  can be fitted by a quadratic function in Eq. (19) (Fig. 4). Substituting the fitting parameters  $a$ ,  $b$ , and  $c$  into Eq. (20), the sensitivity factor that determines the effect degree of the variability of the nondimensional interface toughness  $\Gamma_{TBC}/(E_{TBC}L)$  on the reliability of TBCs is obtained as 1.17. A similar analysis was carried out for thermal strain  $\Delta\alpha\Delta T$  and other variables, and their sensitivity factors on the spallation of an APS ceramic coating are shown in Fig. 5. It is seen that the resistance index of the nondimensional fracture toughness has a significant effect on the reliability of the TBCs, and their difference dominates spallation in the case of load variables (e.g., thermal cycles, growth strain of TGO). It is also indicated that the thermal strain due to the difference in thermal expansion coefficients virtually controls the reliability of the TBCs. These results coincide with

**Table 2** Parameters in probability analysis of TBCs produced by EB-PVD

Property	Mean value	SD	Distribution
$\gamma_F$ (J/m <sup>2</sup> )	50	5	Weibull
$E_{TGO}$ (GPa)	380	100	Weibull
$h$ ( $\mu$ m)	2.85	0.81	Normal
$\Delta\alpha$ ( $10^{-6}/^\circ\text{C}$ )	7.3	0.37	Normal
$\Delta T$ ( $^\circ\text{C}$ )	1080	9.61	Normal

the failure mechanism whereby the thermal mismatch stress (due to thermal expansion coefficient and temperature drop) induces coating spallation.

### 4.2 TBCs by EB-PVD

The EB-PVD ceramic coating has typical columnar grains with a nanometer-scale gap, allowing large strain tolerance during thermal cycling. The ceramic/bond coating interface is much smoother in comparison to that of APS, which results in a relative smaller adhesion capacity. The growth of a TGO at the ceramic/bond interface is widely considered as the key factor to spallation of protective layers. As a ceramicle-like material, the TGO layer shows greater cohesion to the ceramic coating than that of a metal bond coating, and thus, the TGO/metal interface becomes the weak area to produce delamination [37]. The recognized spallation criterion is that the strain energy within the oxide layer is equal to the energy required to produce decohesion at the oxide/bond coating interface. Therefore, the limit state function of interface fail-

ure of TBCs produced by EB-PVD can be expressed as [37]

$$Z = \gamma_F - E_{TGO} (1 - \nu) (\Delta\alpha \Delta T)^2 h = 0, \tag{24}$$

where  $E_{TGO}$  is the Young’s modulus of the TGO,  $\nu$  is Poisson’s ratio,  $h$  is the oxide thickness, and  $\gamma_F$  is the energy required per unit area to produce an interfacial fracture. Based on experimental results [32,38–44], the mean values, deviations, and distributions of parameters in Eq. (24) are given in Table 2. Among these parameters,  $E_{TGO}$  and the parameter  $\gamma_F$  are satisfied by the Weibull distribution, with mean values of 50 J/m<sup>2</sup> and 380 GPa and deviations of 5 J/m<sup>2</sup> and 100 GPa, respectively. The Poisson’s ratio  $\nu$  of the TGO is approximately 0.23. The other parameters are assumed to be normally distributed.

Similarly, the failure probability is estimated by the second-order second moment reliability method. Substituting these parameters into the estimation algorithm, the failure probability of EB-PVD spallation is approximately 46.92%. Figure 6 shows the relationships between the failure probability and the nondimensional variables in Eq. (24). Similar to the results of APS coating, the risk probability decreases with the increase in the nondimensional resistance parameter  $\gamma_F/(E_{TGO}h)$  and increases with the rise of the nondimensional load parameter  $\Delta\alpha\Delta T$ . Fitting these curves with a quadratic function in Eq. (19), the sensitivity factors for EB-PVD coatings can be determined. As shown in Fig. 7, the thermal strain due to the temperature drop and the difference in thermal expansion coefficients virtually control the reliability of the TBCs, which are in good agreement with their failure mechanism [37].

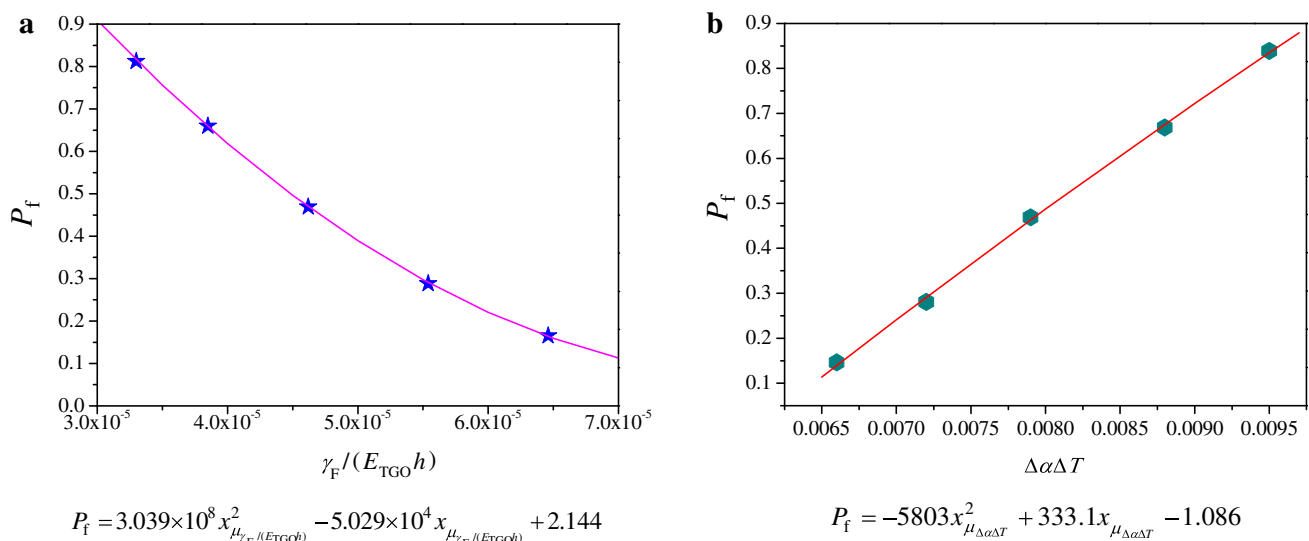


**Fig. 6** Relationships between failure probability and nondimensional variables involved in a limit state function of EB-PVD TBCs: **a** curves of probability vs.  $\gamma_F/(E_{TGO}h)$ ; **b** curves of probability vs.  $\Delta\alpha\Delta T$



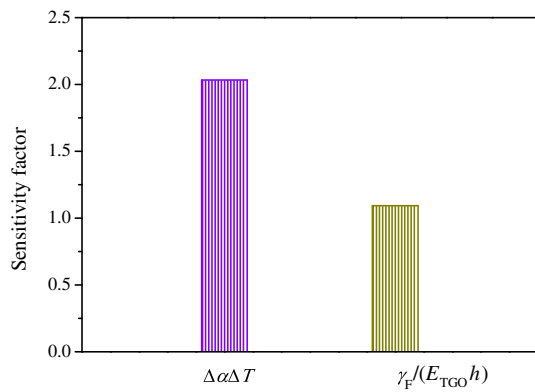


**Fig. 7** Sensitivity factors of nondimensional variables in spallation of EB-PVD ceramic coating

It is worth noting that the accuracy of the parameters of TBCs is important for the reliability assessment. Though the parameters used in this work fall within a reasonable range, we must admit that our work is incomplete. The result should only be compared with experiments conducted to ascertain precision. We are still working on the collection and measurement of reasonable parameters to improve the reliability assessment.

## 5 Conclusions

A reliability assessment method for the interface failure of TBCs has been established based on a failure probability analysis. The interface failure of two kinds of TBC with different mechanisms was analyzed. It is shown that the failure probabilities are 40.64% and 46.92%, indicating that these TBCs cannot meet design requirements under severe circumstances. For both TBCs, the temperature drop of load-related parameters and the thermal mismatch in material-related parameters mainly control their reliabilities. Under temperature cycling, the load can be regarded as the product of thermal mismatch and temperature drop, and thus the load-related parameters have a more significant effect on the uncertainty of service reliability in comparison to material or geometry-related parameters. It is also shown that reliability can be improved by increasing the resistance index of TBCs. Therefore, such a methodology provides a quantitative way to assess the risk level and further tailor specific designs with a given reliability.

**Acknowledgments** This work was supported by the National Natural Science Foundation of China (Grants 11002122, 51172192, and 11272275), the Military-Civil Special Foundation of Hunan Province (Grant 2013280), the Natural Science Foundation of Hunan Province (Grant 11JJ4003), and the Doctoral Scientific Research Foundation of Xiangtan University (Grants KZ08022, KZ03013, and KF20140303).

## References

1. Beele, W., Marijnissen, G., Van, L.A.: The evolution of thermal barrier coatings—status and upcoming solutions for today's key issues. *Surf. Coat. Technol.* **120**, 61–67 (1999)
2. Padture, N.P., Gell, M., Jordan, E.H.: Thermal barrier coatings for gas-turbine engine applications. *Science* **296**, 280–284 (2002)
3. Evans, A.G., Mumm, D.R., Hutchinson, J.W., et al.: Mechanisms controlling the durability of thermal barrier coatings. *Prog. Mater. Sci.* **46**, 505–553 (2001)
4. Miller, R.A.: Current status of thermal barrier coatings—an overview. *Surf. Coat. Technol.* **30**, 1–11 (1987)
5. Sørensen, K.D., Jensen, H.M.: Buckling-driven delamination in layered spherical shells. *J. Mech. Phys. Solids* **56**, 230–240 (2008)
6. Jensen, H.M., Sheinman, I.: Numerical analysis of buckling-driven delamination. *Int. J. Solids Struct.* **39**, 3373–3386 (2002)
7. Busso, E.P., Lin, J., Sakurai, S.: A mechanistic study of oxidation-induced degradation in a plasma-sprayed thermal barrier coating system.: Part II: life prediction model. *Acta Mater.* **49**, 1529–1536 (2001)
8. Busso, E.P., Wright, L., Evans, H.E., et al.: A physics-based life prediction methodology for thermal barrier coating systems. *Acta Mater.* **55**, 1491–1503 (2007)
9. Renusch, D., Schütze, M.: Measuring and modeling the TBC damage kinetics by using acoustic emission analysis. *Surf. Coat. Technol.* **202**, 740–744 (2007)
10. Beck, T., Herzog, R., Trunova, O.: Damage mechanisms and lifetime behavior of plasma-sprayed thermal barrier coating systems for gas turbines—part II: modeling. *Surf. Coat. Technol.* **202**, 5901–5908 (2008)
11. Yang, L., Zhong, Z.C., Zhou, Y.C.: Quantitative assessment of the surface crack density in thermal barrier coatings. *Acta Mech. Sin.* **30**, 167–174 (2014)
12. Barber, B., Jordan, E., Gell, M., et al.: Assessment of damage accumulation in thermal barrier coatings using a fluorescent dye infiltration technique. *J. Therm. Spray Technol.* **8**, 79–86 (1999)
13. He, M.Y., Hutchinson, J.W., Evans, A.G.: Simulation of stresses and delamination in a plasma-sprayed thermal barrier system upon thermal cycling. *Mater. Sci. Eng. A* **345**, 172–178 (2003)
14. Tzimas, E., Müllejans, H., Petevs, S.D., et al.: Failure of thermal barrier coating systems under cyclic thermomechanical loading. *Acta Mater.* **48**, 4699–4707 (2000)
15. Meier, S.M., Sheffler, K.D., Nissley, D.M.: Thermal barrier coating life prediction model development, phase 2. Final report, Pratt and Whitney Aircraft, East Hartford (1991)
16. Guo, S.Q., Kagawa, Y.: Effect of thermal exposure on hardness and Young's modulus of EB-PVD yttria-partially-stabilized zirconia thermal barrier coatings. *Ceram. Int.* **32**, 263–270 (2006)
17. Bhatnagar, H.S., Ghosh, S., Walter, M.E.: Parametric studies of failure mechanisms in elastic EB-PVD thermal barrier coatings using FEM. *Int. J. Solids Struct.* **43**, 4384–4406 (2006)
18. Yang, L., Zhou, Y.C., Mao, W.G., et al.: Real-time acoustic emission testing based on wavelet transform for the failure process of thermal barrier coatings. *Appl. Phys. Lett.* **93**, 231906 (2008)
19. Yang, L., Zhou, Y.C., Lu, C.S.: Damage evolution and rupture time prediction in thermal barrier coatings subjected to cyclic heating and cooling: an acoustic emission method. *Acta Mater.* **59**, 6519–6529 (2011)
20. Chen, X., He, M.Y., Spitsberg, I., et al.: Mechanisms governing the high temperature erosion of thermal barrier coatings. *Wear* **256**, 735–746 (2004)
21. Mercer, C., Faulhaber, S., Evans, A.G., et al.: A delamination mechanism for thermal barrier coatings subject to calcium-magnesium-alumino-silicate (CMAS) infiltration. *Acta Mater.* **53**, 1029–1039 (2005)

22. Rackwitz, R.: Reliability analysis—a review and some perspectives. *Struct. Saf.* **23**, 365–395 (2001)
23. Madsen, H.O., Krenk, S., Lind, N.C.: *Methods of Structural Safety*. Courier Corporation, Mineola (2006)
24. Köyliüoğlu, H.U., Nielsen, S.R.: New approximations for SORM integrals. *Struct. Saf.* **13**, 235–246 (1994)
25. Lopes, P.A.M., Gomes, H.M., Awruch, A.M.: Reliability analysis of laminated composite structures using finite elements and neural networks. *Compos. Struct.* **92**, 1603–1613 (2010)
26. Mori, Y., Ellingwood, B.R.: Time-dependent system reliability analysis by adaptive importance sampling. *Struct. Saf.* **12**, 59–73 (1993)
27. Rajashekhar, M.R., Ellingwood, B.R.: A new look at the response surface approach for reliability analysis. *Struct. Saf.* **12**, 205–220 (1993)
28. Breitung, K.: Asymptotic approximations for multinormal integrals. *J. Eng. Mech.* **110**, 357–366 (1984)
29. Zhao, G.F.: *Reliability Theory and Its Applications for Engineering Structures*, pp. 302–303. Dalian University of Technology Press, Dalian (1996)
30. Wu, H.S., Zhong, Q.P.: Assessment for integrity of structures containing defects. *Int. J. Pres. Ves. Pip.* **75**, 343–346 (1998)
31. Martena, M., Botto, D., Fino, P., et al.: Modelling of TBC system failure: stress distribution as a function of TGO thickness and thermal expansion mismatch. *Eng. Fail. Anal.* **13**, 409–426 (2006)
32. Murthy, P.L., Nemeth, N.N., Brewer, D.N., et al.: Probabilistic analysis of a SiC/SiC ceramic matrix composite turbine vane. *Compos. Part B-Eng.* **39**, 694–703 (2008)
33. Danzer, R., Supancic, P., Pascual, J., et al.: Fracture statistics of ceramics-Weibull statistics and deviations from Weibull statistics. *Eng. Fract. Mech.* **74**, 2919–2932 (2007)
34. Wan, J., Zhou, M., Yang, X.S., et al.: Fracture characteristics of freestanding 8 wt.%  $Y_2O_3$ - $ZrO_2$  coatings by single edge notched beam and vickers indentation tests. *Mater. Sci. Eng. A* **581**, 140–144 (2013)
35. Shen, W., Wang, F.C., Fan, Q.B., et al.: Finite element simulation of tensile bond strength of atmospheric plasma spraying thermal barrier coatings. *Surf. Coat. Technol.* **205**, 2964–2969 (2011)
36. Mao, W.G., Dai, C.Y., Yang, L., et al.: Interfacial fracture characteristic and crack propagation of thermal barrier coatings under tensile conditions at elevated temperatures. *Int. J. Fract.* **151**, 107–120 (2008)
37. Evans, H.E.: Oxidation failure of TBC systems: an assessment of mechanisms. *Surf. Coat. Technol.* **206**, 1512–1521 (2011)
38. Taylor, M.P., Jackson, R.D., Evans, H.E.: The effect of bond coat oxidation on the microstructure and endurance of a thermal barrier coating system. *Mater. High Temp.* **26**, 317–323 (2009)
39. Sfar, K., Aktaa, J., Munz, D.: Numerical investigation of residual stress fields and crack behavior in TBC systems. *Mater. Sci. Eng. A* **333**, 351–360 (2002)
40. Guo, S.Q., Kagawa, Y.: Young's moduli of zirconia top-coat and thermally grown oxide in a plasma-sprayed thermal barrier coating system. *Scr. Mater.* **50**, 1401–1406 (2004)
41. Ma, K.K., Schoenung, J.M.: Isothermal oxidation behavior of cryomilled NiCrAlY bond coat: homogeneity and growth rate of TGO. *Surf. Coat. Technol.* **205**, 5178–5185 (2011)
42. Che, C., Wu, G.Q., Qi, H.Y.: Uneven growth of thermally grown oxide and stress distribution in plasma-sprayed thermal barrier coatings. *Surf. Coat. Technol.* **203**, 3088–3091 (2009)
43. Shen, W., Wang, F.C., Fan, Q.B.: Lifetime prediction of plasma-sprayed thermal barrier coating systems. *Surf. Coat. Technol.* **217**, 39–45 (2013)
44. Tomimatsu, T., Zhu, S., Kagawa, Y.: Effect of thermal exposure on stress distribution in TGO layer of EB-PVD TBC. *Acta Mater.* **51**, 2397–2405 (2003)